JACS
JOURNAL OF THE AMERICAN CHEMICAL SOCIETY
Article
Cite This: J. Am. Chem. Soc. 2018, 140, 3412−3422
pubs.acs.org/JACS

Separation of Xylene Isomers through Multiple Metal Site Interactions in Metal−Organic Frameworks

Miguel I. Gonzalez,[†,○] Matthew T. Kapelewski,[†,○] Eric D. Bloch,[†,#] Phillip J. Milner,[†] Douglas A. Reed,[†] Matthew R. Hudson,[§] Jarad A. Mason,[†,▽] Gokhan Barin,[†] Craig M. Brown,[§,∥] and Jeffrey R. Long*[,†,‡,⊥]

[†]Department of Chemistry, and [‡]Department of Chemical Engineering, University of California, Berkeley, California 94720, United States

[§]Center for Neutron Research, National Institute of Standards and Technology, Gaithersburg, Maryland 20899, United States

[∥]Chemical and Biomolecular Engineering, University of Delaware, Newark, Delaware 19716, United States

[⊥]Materials Sciences Division, Lawrence Berkeley National Laboratory, Berkeley, California 94720, United States

Supporting Information

ABSTRACT: Purification of the C_8 alkylaromatics *o*-xylene, *m*-xylene, *p*-xylene, and ethylbenzene remains among the most challenging industrial separations, due to the similar shapes, boiling points, and polarities of these molecules. Herein, we report the evaluation of the metal−organic frameworks Co_2(dobdc) (dobdc^{4-} = 2,5-dioxido-1,4-benzenedicarboxylate) and Co_2(*m*-dobdc) (*m*-dobdc^{4-} = 4,6-dioxido-1,3-benzenedicarboxylate) for the separation of xylene isomers using single-component adsorption isotherms and multicomponent breakthrough measurements. Remarkably, Co_2(dobdc) distinguishes among all four molecules, with binding affinities that follow the trend *o*-xylene > ethylbenzene > *m*-xylene > *p*-xylene. Multicomponent liquid-phase adsorption measurements further demonstrate that Co_2(dobdc) maintains this selectivity over a wide range of concentrations. Structural characterization by single-crystal X-ray diffraction reveals that both frameworks facilitate the separation through the extent of interaction between each C_8 guest molecule with two adjacent cobalt(II) centers, as well as the ability of each isomer to pack within the framework pores. Moreover, counter to the presumed rigidity of the M_2(dobdc) structure, Co_2(dobdc) exhibits an unexpected structural distortion in the presence of either *o*-xylene or ethylbenzene that enables the accommodation of additional guest molecules.

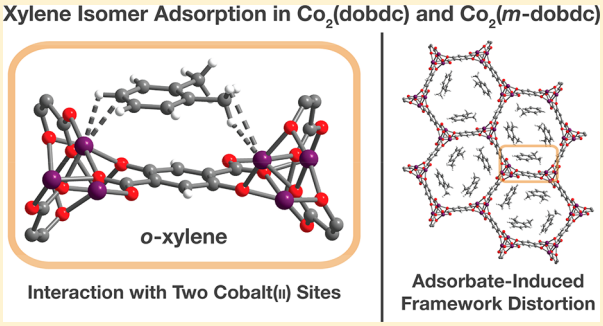

INTRODUCTION

Industrial chemical separations account for 15% of the global energy demand.[1] As a consequence, the development of more energy-efficient separations using adsorbent- or membrane-based technologies represents a key pursuit toward mitigating the continuous rise in worldwide energy consumption.[1] One of the most difficult industrial mixtures to partition consists of the C_8 isomers *o*-xylene, *m*-xylene, *p*-xylene, and ethylbenzene, which are primarily obtained from either reformates or pyrolysis gasoline.[2] Both sources yield mixtures of the four isomers that do not match market demand. For example, of the 39.2 Mt of xylenes produced in 2008, 33.0 Mt was used as pure *p*-xylene, 3.6 Mt as *o*-xylene, 0.4 Mt as *m*-xylene, and the remainder was used directly without separation as mixed xylenes solvent.[3] The large need for pure *p*-xylene stems from its use as a precursor to terephthalic acid, a major feedstock in the production of polyesters and polyamides.[4] The second most valuable isomer, *o*-xylene, is mainly converted to phthalic anhydride, a precursor to plasticizers.[5] Current processes do not isolate ethylbenzene from the C_8 mixture, as the isomer is produced more economically by the alkylation of benzene with ethylene.[6] Optimizing output to meet economic demand requires separation of the desired isomers, mainly *p*-xylene and some *o*-xylene, followed by isomerization of the unwanted fraction back to the thermodynamic mixture.[2]

The similar boiling points of the C_8 isomers make distillative separation of all four nearly impossible, while their comparable sizes and polarizabilities limit the ability of adsorbents to distinguish between the different isomers (Table 1). Current state-of-the-art technology involves either crystallization (25%

Table 1. Physical Properties of the C_8 Alkylaromatics[2,7]

C_8 isomer	boiling point (°C)	kinetic diameter (Å)	dipole moment ($\times 10^{18}$ esu cm)	polarizability ($\times 10^{-25}$ cm^3)
o-xylene	144.4	6.8	0.649	141−149
m-xylene	139.1	6.8	0.36	142
p-xylene	138.4	5.8	0.1	137−149
ethylbenzene	136.2	5.8	0.59	142

Received: December 31, 2017
Published: February 15, 2018

DOI: 10.1021/jacs.7b13825
J. Am. Chem. Soc. 2018, 140, 3412−3422

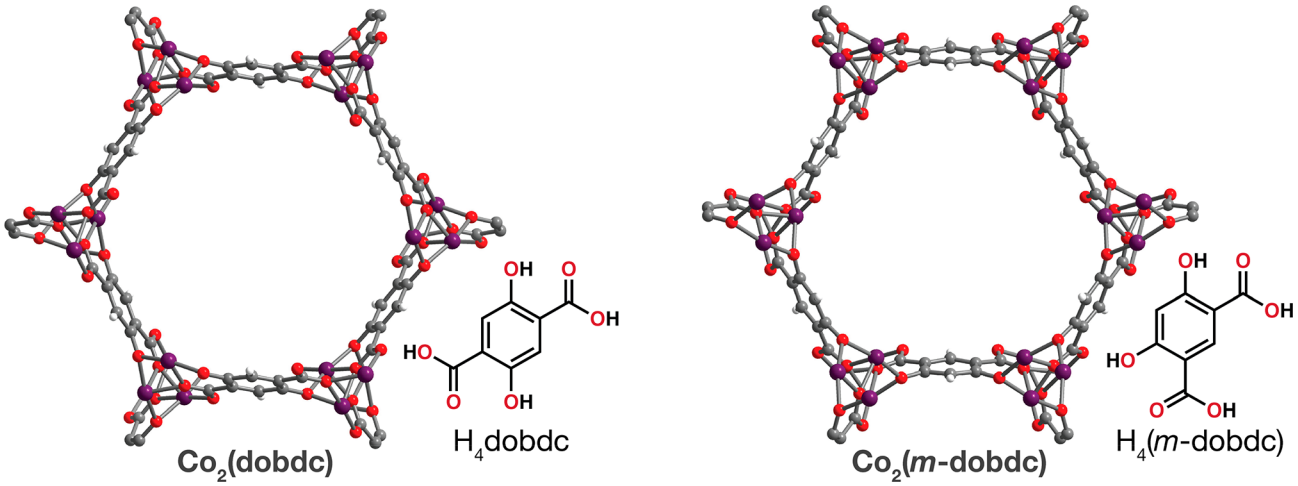

Figure 1. A portion of the crystal structures of Co_2(dobdc) and Co_2(*m*-dobdc) (dobdc^{4-} = 2,5-dioxido-1,4-benzenedicarboxylate; *m*-dobdc^{4-} = 4,6-dioxido-1,3-benzenedicarboxylate); purple, red, gray, and white spheres represent Co, O, C, and H atoms, respectively.

of production) or adsorption (75% of production) to effect separation. Industrial adsorption-based techniques for the production of pure *p*-xylene are carried out in the liquid phase with faujasite-type zeolites using simulated moving bed technology.[4] Although difficult, *o*-xylene can be separated by fractional distillation, while the *m*-xylene and ethylbenzene are obtained through other adsorption- and complexation-based processes, such as the commonly used Parex process from Honeywell UOP.[8] The isolation of all four isomers using a single process has yet to be implemented, prompting research efforts to pursue the development of more efficient technologies. Several studies have focused on improving adsorptive separations with zeolites,[9−13] while more recent work has highlighted membrane-based separations as competitive and less energy-intensive alternatives.[9,14]

Metal−organic frameworks have previously been studied for the separation of hydrocarbon mixtures such as ethane/ethylene, propane/propylene, and C_6 alkane mixtures, among many others.[15] In particular, some of these materials have been studied for the separation of xylene isomers based on size and shape selectivity.[9,16−29] For example, frameworks with small pore apertures, such as Zn(2-methylimidazolate)$_2$ or ZIF-8[16] and Zn([1,1′-biphenyl]-3,5-dicarboxylate),[17] have been shown to selectively adsorb *p*-xylene over *o*-xylene and *m*-xylene due to its smaller kinetic diameter. In addition, the framework V(O)(bdc) (H_2bdc = 1,4-benzenedicarboxylic acid) or MIL-47 affords separation based on packing differences and adsorbate−adsorbate interactions upon adsorption,[19] engendering many follow-up studies on both MIL-47[20,21] and its structural analogues M(OH)(bdc) or MIL-53-M (M = Al, Fe).[22,28,29] Finally, the flexible metal−organic framework Ce(Htcpb) (H_4tcpb = 1,2,4,5-tetrakis(4-carboxyphenyl)-benzene) has been demonstrated to separate the four C_8 isomers effectively through shape-selective conformational changes in response to specific isomers.[27]

Frameworks bearing coordinatively unsaturated metal centers have been extensively investigated as adsorbents for the separations of small gas molecules, due to the ability of their exposed metal sites to bind specific gases preferentially.[15,30−41] Despite considerable work demonstrating the ability of these materials to separate gas mixtures that are generally difficult to purify, only a limited number of studies have explored their use in the separation of larger molecules such as the C_8 alkylaromatics.[19,26] In one report, the metal−organic framework Ni_2(dobdc) was shown to separate two-component mixtures of *o*-xylene, *m*-xylene, and *p*-xylene, although the exposed nickel(II) coordination sites in this material were thought to play a minor role in the separation.[26] Here, we demonstrate through adsorption and breakthrough measurements coupled with structural characterization by single-crystal X-ray diffraction that the metal−organic frameworks Co_2(dobdc) and Co_2(*m*-dobdc) (Figure 1) facilitate the separation of the C_8 aromatics through subtle differences in the interaction of two coordinatively unsaturated metal centers with each C_8 molecule. Furthermore, Co_2(dobdc) is found to undergo a structural distortion upon binding either *o*-xylene or ethylbenzene, which significantly increases its adsorption capacity for these isomers.

EXPERIMENTAL SECTION

Materials and Methods. *N*,*N*-Dimethylformamide (DMF), tetrahydrofuran (THF), ethanol, and methanol were obtained from commercial sources and used without further purification. The solvent *n*-heptane, the internal standard *n*-undecane, and the C_8 isomers *o*-xylene, *m*-xylene, *p*-xylene, and ethylbenzene were purchased from commercial sources, dried over sodium (*n*-heptane) or 3 Å molecular sieves (undecane, *o*-xylene, *m*-xylene, *p*-xylene, and ethylbenzene), degassed via three successive freeze−pump−thaw cycles, and then stored over 3 Å molecular sieves in an N_2-filled glovebox. The compounds $Co(NO_3)_2{\cdot}6H_2O$, Co(acetate)$_2{\cdot}4H_2O$, and 2,5-dihydroxy-1,4-benzenedicarboxylic acid (H_4dobdc) were purchased from commercial sources and used as received. The metal−organic framework Co_2(dobpdc) (dobpdc^{4-} = 4,4′-dioxidobiphenyl-3,3′-dicarboxylate), which is the expanded analogue of Co_2(dobdc), and the ligand 4,4′-dioxidobiphenyl-3,3′-dicarboxylic acid (H_4dobpdc) were synthesized according to a previously published procedure as detailed in the Supporting Information.[42]

Synthesis of H_4(*m*-dobdc). Resorcinol (1,3-dihydroxybenzene; 37.6 g, 0.340 mol) and $KHCO_3$ (100 g, 1.00 mmol) were pulverized separately and dried under vacuum. The two powders were then mixed together thoroughly and placed in a glass jar that was sealed in a Parr reaction bomb equipped with an internal thermocouple and a pressure gauge. The reaction bomb was evacuated under vacuum and then dosed with CO_2 to 40 bar pressure. The bomb was heated to 250 °C (as measured by the internal thermocouple) in a sand bath for 24 h and then slowly cooled to room temperature. The pressure was vented and 1 L of water was added to the solid in the jar, which was broken up mechanically, followed by sonication of the mixture. The resulting suspension was filtered, and the filtrate was acidified with 12 M HCl

DOI: 10.1021/jacs.7b13825
J. Am. Chem. Soc. 2018, 140, 3412−3422

until reaching a pH < 2, at which point white solid H_4(*m*-dobdc) had precipitated. The solid product was collected by filtration. Yield: 53.2 g, 79%. ^{1}H NMR (400 MHz, DMSO-d_6) δ 9.22 ppm (br, 4H), 8.28 ppm (s, 1H), 6.22 ppm (s, 1H); ^{13}C NMR (400 MHz, DMSO-d_6) δ 172.0 ppm, 167.7 ppm, 134.3 ppm, 107.3 ppm, 103.0 ppm.

Synthesis of Co_2(dobdc). The framework Co_2(dobdc) was synthesized using a slight modification to a previously published procedure.[30] A 1 L Pyrex jar was charged with H_4dobdc (2.23 g, 11.3 mmol), $Co(NO)_2{\cdot}6H_2O$ (10.9 g, 37.5 mmol), and a 1:1:1 (v/v/v) mixture of DMF/ethanol/water (900 mL), and then sealed with a PTFE-lined cap. The resulting mixture was sonicated until all reactants were fully dissolved to form a violet solution. The reaction mixture was then placed in an oven that was preheated to 100 °C and kept at this temperature for 24 h, yielding violet needle-shaped single crystals. The crystals were soaked three times in 1 L of DMF for 24 h at 120 °C, followed by soaking three times in 1 L of methanol at 60 °C. The crystals were then heated at 180 °C under dynamic vacuum for 24 h to give fully desolvated Co_2(dobdc). Langmuir surface area (N_2, 77 K): 1410 m^2/g.

The single crystals obtained from the large-scale synthesis of Co_2(dobdc) were all found to exhibit obverse/reverse twinning, which complicated analysis of the structures showing distortion of the lattice upon soaking with *o*-xylene or ethylbenzene. Nontwinned single crystals were therefore synthesized using a slight modification to a previously published procedure.[43] A solution of H_4dobdc (74.3 mg, 0.375 mmol) in 2.5 mL of THF was added to a solution of $Co(acetate)_2{\cdot}4H_2O$ (93.4 mg, 0.375 mmol) in 2.5 mL of deionized water in a PTFE-lined Parr-reactor. The reactor was placed in an oven that was preheated to 110 °C and kept at this temperature for 5 days to give pink needle-shaped single crystals. The crystals were soaked three times in 20 mL of DMF for 24 h at 120 °C, followed by soaking three times in 20 mL of methanol at 60 °C. Fully desolvated Co_2(dobdc) single crystals were obtained by heating at 180 °C under dynamic vacuum for 24 h.

Synthesis of Co_2(*m*-dobdc). The framework Co_2(*m*-dobdc) was synthesized according to literature procedures.[44] A 1 L three-neck round-bottom flask was charged with 310 mL of methanol and 310 mL of DMF and sparged with N_2 for 1 h while stirring. The solids H_4(*m*-dobdc) (2.00 g, 10.1 mmol) and $CoCl_2$ (3.27 g, 25.2 mmol) were added, and the flask was equipped with a reflux condenser and sealed under N_2, forming a blue-pink suspension. The reaction mixture was then stirred at 120 °C for 18 h, yielding a pink microcrystalline solid that was isolated by filtration. The powder was soaked in 500 mL of DMF at 60 °C for 24 h, followed by soaking three times in 500 mL of methanol at 60 °C for 24 h. The resulting powder was collected by filtration and heated to 180 °C under dynamic vacuum for 24 h to give fully desolvated Co_2(*m*-dobdc). Langmuir surface area (N_2, 77 K): 1500 m^2/g.

Single crystals of Co_2(*m*-dobdc) were prepared by adapting the procedure used for the large-scale synthesis of Co_2(dobdc). A 100 mL Pyrex jar was charged with H_4(*m*-dobdc) (198 mg, 1.00 mmol), $Co(NO)_2{\cdot}6H_2O$ (970 mg, 3.33 mmol), and 80 mL of a 1:1:1 (v/v/v) mixture of DMF/ethanol/water, and then sealed with a PTFE-lined cap. The resulting mixture was sonicated until all reactants were fully dissolved to form a pink solution. The reaction mixture was then placed in an oven that was preheated to 100 °C and kept at this temperature for 24 h, yielding pink needle-shaped single crystals. The crystals were soaked three times in 100 mL of DMF at 120 °C for 24 h, followed by soaking three times in 100 mL of methanol at 60 °C. Fully desolvated Co_2(*m*-dobdc) single crystals were obtained by heating at 180 °C under dynamic vacuum for 24 h.

Single-Component Vapor-Phase Adsorption Experiments. Approximately 150 mg of each sample was loaded into a preweighed sample tube in an N_2-filled glovebox, and the sample tubes were capped with a Transeal equipped with Kalrez O-rings. The samples were then transferred to a Micromeritics 2420 instrument degas manifold and heated at a rate of 0.2 °C/min to a temperature of 180 °C while each sample was under vacuum. When a degas rate of <1 μbar/min was achieved, each sample was considered to be activated. Following this procedure, the samples were transferred to a Micromeritics 3Flex gas adsorption analyzer equipped with a vapor dosing tube for single-component xylene adsorption measurements. Each sample tube was subsequently immersed in a temperature-controlled oil bath that surrounded most of the tube. Each xylene was stored over 3 Å molecular sieves prior to being placed in the vapor dosing tube, and was degassed on the instrument via three freeze–pump–thaw cycles. The vapor dosing tube was then heated to 35 °C with a heating mantle and kept at this temperature for the duration of the experiment. The manifold of the instrument itself was heated to 45 °C to prevent condensation of liquid xylenes. Experiments were conducted with the instrument in fixed pressure incremental dose mode in increments of 0.1 mmol/g. Importantly, to ensure full equilibration of each isomer with the metal–organic framework adsorbent, each dose was allowed to equilibrate until the change in pressure was below 0.01% of the average pressure measured over a 90 s interval.

Multicomponent Vapor-Phase Breakthrough Experiments. Qualitative breakthrough experiments were carried out using a custom-built breakthrough apparatus consisting of Swagelok fittings and copper tubing connecting an N_2 cylinder, several valves, a sample holder, and a bubbler to a PerkinElmer Clarus 500 gas chromatograph (GC). A mixture of *o*-xylene, *m*-xylene, *p*-xylene, and ethylbenzene was loaded into a glass bubbler connected to the setup. Nitrogen (N_2, 99.999%) was flowed through the bubbler at a rate of 40 mL/min, which was controlled by a Parker Porter mass flow controller. The composition of the four components in the bubbler was adjusted until a 1:1:1:1 mixture was achieved in the vapor phase, as detected by the GC equipped with a Supelco SCOT Bentone 34/DNDP capillary column. Each sample was then loaded into one vertical portion of a U-shaped Swagelok assembly equipped with a fritted gasket to hold the sample in place, and then connected to the apparatus and heated to 125 °C. The C_8 mixture from the bubbler was carried by this nitrogen flow through the sample and to the GC, which sampled the effluent gas every 5 min. Peak integration of each sampling event allowed for the determination of the relative amounts of each component over time.

Multicomponent Liquid-Phase Adsorption Experiments. In an N_2-filled glovebox, equimolar stock solutions of *o*-xylene, *m*-xylene, *p*-xylene, and ethylbenzene (0.010–1.7 M for each isomer) in dry *n*-heptane were prepared with *n*-undecane (0.01 M) as an internal standard. For each concentration, a 250 μL aliquot of C_8 isomer solution was added to a preweighed (~20 mg in most cases) sample of Co_2(dobdc) in a 4 mL vial. Each sample vial was sealed with a PTFE-lined cap and kept at 33 °C for 24 h. The concentrations of both the stock solution and the solution over the Co_2(dobdc) were both analyzed by gas chromatography using an SRI instruments 8610 V GC equipped with a Supelco SCOT Bentone 34/DNDP capillary column and a Cobra autosampler. The amount of each isomer adsorbed was then calculated from the difference between the initial and equilibrium concentrations of the isomer and the mass of the Co_2(dobdc) sample. Two-component selectivities, *S*, were calculated according to eq 1, where q_i and q_j represent the quantities adsorbed for components *i* and *j*, respectively, while C_i and C_j represent the equilibrium concentrations for components *i* and *j*, respectively.

$$S = \frac{q_i/q_j}{C_i/C_j} \tag{1}$$

Single-Crystal X-ray Diffraction. In an N_2-filled glovebox, fully desolvated single crystals of either Co_2(dobdc) or Co_2(*m*-dobdc) were soaked in ~3 mL of *o*-xylene, *m*-xylene, *p*-xylene, or ethylbenzene for at least 24 h at 33 °C in 4 mL vials sealed with PTFE-lined caps. Sample vials were kept sealed and taken out of the glovebox prior to data collection. Immediately after opening the sample vial, crystals were coated with Paratone-N oil, mounted on MiTeGen loops, and then cooled to 100 K using an Oxford Cryostreams cryostream for data collection. X-ray diffraction data for all samples were collected at Beamline 11.3.1 at the Advanced Light Source at Lawrence Berkeley National Laboratory using synchrotron radiation (λ = 0.8856 Å for Co_2(dobdc)·0.99(*o*-xylene), Co_2(dobdc)·0.36(ethylbenzene),

DOI: 10.1021/jacs.7b13825
J. Am. Chem. Soc. 2018, 140, 3412–3422

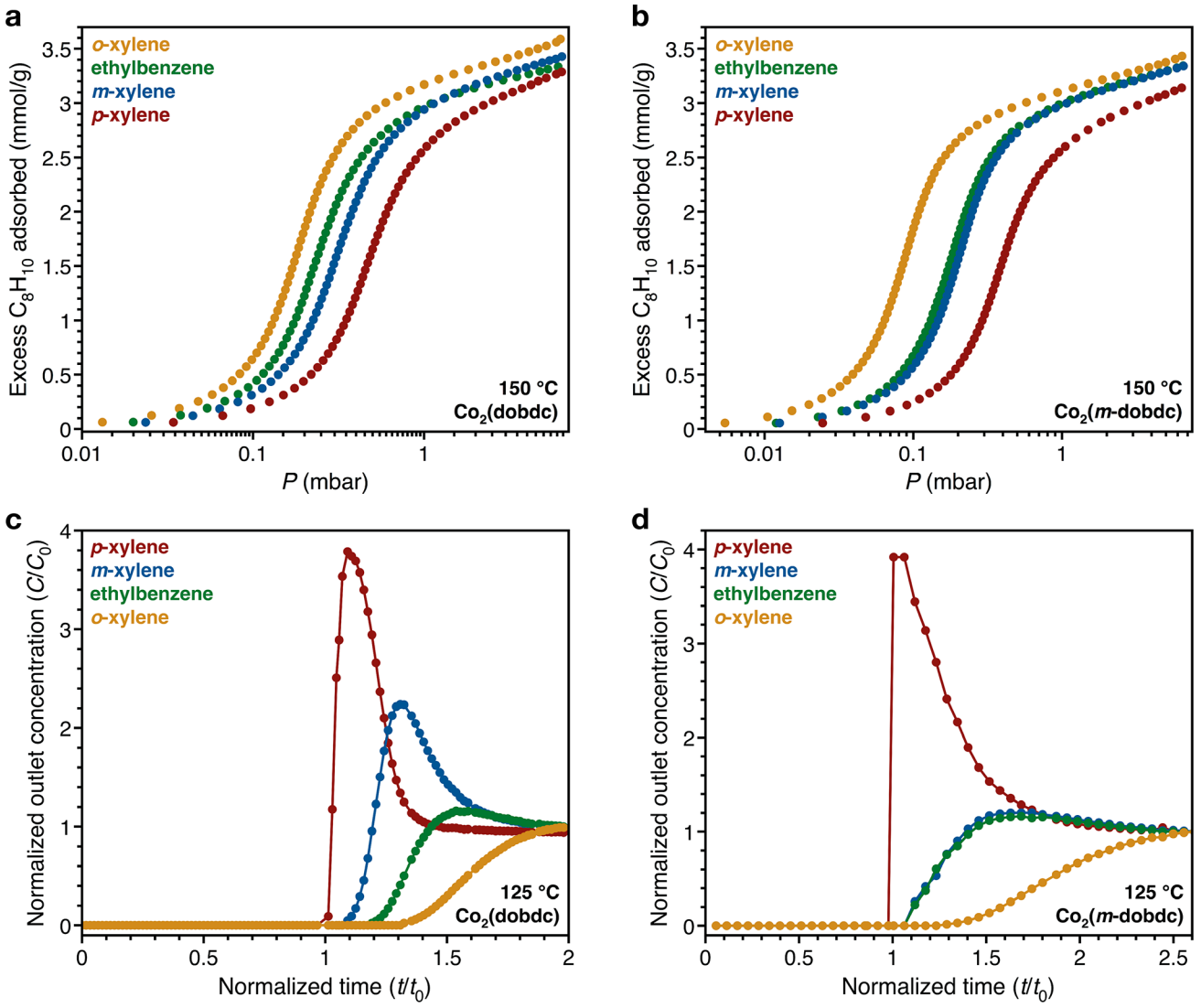

Figure 2. Single-component vapor-phase *o*-xylene (yellow), ethylbenzene (green), *m*-xylene (blue), and *p*-xylene (red) adsorption isotherms for Co_2(dobdc) (a) and Co_2(*m*-dobdc) (b) at 150 °C. Multicomponent vapor-phase breakthrough measurements for an equimolar mixture of *o*-xylene (yellow), ethylbenzene (green), *m*-xylene (blue), and *p*-xylene (red) vapor with Co_2(dobdc) (c) and Co_2(*m*-dobdc) (d) at 125 °C. To facilitate comparisons between the two breakthrough experiments, time is normalized by assigning the time of *p*-xylene breakthrough as t_0.

Co_2(dobdc)·0.82(*p*-xylene), and Co_2(*m*-dobdc)$(H_2O)_{0.61}$·0.77-(ethylbenzene); λ = 0.7749 Å for Co_2(dobdc)·0.74(*m*-xylene) and Co_2(*m*-dobdc)·0.92(*o*-xylene)) with a Bruker D8 diffractometer equipped with a Bruker PHOTON100 CMOS detector.

Raw data were integrated and corrected for Lorentz and polarization effects using Bruker AXS SAINT[45] software and corrected for absorption using SADABS.[46] The structures were solved using direct methods with SHELXS[47,48] or intrinsic phasing using SHELXT[49] and refined using SHELXL[47,50] operated in the OLEX2 interface.[51] Thermal parameters were refined anisotropically for all non-hydrogen atoms. In all structures, disorder of the C_8 isomers required the use of displacement parameter and distance restraints. In some cases, the disorder was so severe that geometric constraints were necessary to model the aromatic ring of the C_8 isomers. All hydrogen atoms were refined using the riding model. In the presence of either *o*-xylene or ethylbenzene, Co_2(dobdc) undergoes a structural distortion that involves the elongation of three out of four hexagonal channels along the direction normal to two opposing walls of the pore. This distortion results in the formation of a supercell, characterized by the doubling of both the *a* and *b* axes of the undistorted structure. Refinement of the distorted structures (Co_2(dobdc)·0.99(*o*-xylene) and Co_2(dobdc)·0.36(ethylbenzene)) revealed significant residual electron density at positions that match the structure of the undistorted framework (Figures S10 and S11), suggesting that a small fraction of these crystals remain undistorted. This likely arises from defects in the crystals where the cobalt(II) sites are inaccessible, which has been reported in the M_2(dobdc) series of metal−organic frameworks based on gas adsorption measurements.[35] A suitable structural model that accounts for this electron density could not be generated, leading to high *R*-factors for both structures.

RESULTS AND DISCUSSION

C_8 Isomer Adsorption Experiments. The isomeric metal−organic frameworks Co_2(dobdc) and Co_2(*m*-dobdc) both possess one-dimensional hexagonal channels lined with a high density of coordinatively unsaturated cobalt(II) centers.[30,44] To determine the ability of these frameworks to distinguish the four C_8 isomers, single-component adsorption isotherms were collected at 150 °C. Comparison of the adsorption isotherms for Co_2(dobdc) (Figure 2a) reveals that the affinity of the framework for each isomer follows the trend *o*-xylene > ethylbenzene > *m*-xylene > *p*-xylene, suggesting that all four molecules can be separated by the framework. In

DOI: 10.1021/jacs.7b13825
J. Am. Chem. Soc. 2018, 140, 3412−3422

contrast, the order of adsorption strength in Co_2(*m*-dobdc) is *o*-xylene > ethylbenzene ≈ *m*-xylene > *p*-xylene (Figure 2b), which indicates that the framework cannot discriminate between ethylbenzene and *m*-xylene despite having a structure similar to that of Co_2(dobdc). Previous work has shown that Ni_2(dobdc) exhibits the same trend in affinity for *o*-xylene, *m*-xylene, and *p*-xylene.[26] Both cobalt frameworks show saturation capacities that range from 3.1−3.6 mmol/g at ∼7 mbar, which are much higher than those reported for the Ni variant (1.9−2.1 mmol/g), and correspond to the adsorption of one xylene molecule per two metal centers (3.2 mmol/g). Notably, Co_2(dobdc) and Co_2(*m*-dobdc) also display greater volumetric capacities (3.8−4.2 mmol/cm^3) than those reported for the industrially relevant faujasite-type zeolites (2.4−2.8 mmol/cm^3 for NaY).[4,26,52,53] In general, the adsorption isotherms for the C_8 isomers in Co_2(dobdc) and Co_2(*m*-dobdc) show considerable uptake at low pressures (0.1 to 1 mbar) and relatively high temperature, indicating strong interactions between the framework and the alkylaromatics.

Additional single-component isotherms were collected at 140 and 160 °C (Figures S18 and S19) for each C_8 isomer in both frameworks to determine differential enthalpies of adsorption. These were found to range from −63 ± 4 kJ/mol for ethylbenzene to −77 ± 6 kJ/mol for *o*-xylene in Co_2(dobdc), and from −67 ± 2 kJ/mol for *p*-xylene to −81 ± 1 kJ/mol for ethylbenzene in Co_2(*m*-dobdc) at about half saturation capacity (Figure S20). The adsorption isotherm data at 140, 150, and 160 °C were not of sufficient quality to obtain accurate differential enthalpies of adsorption. As a result, the large errors associated with the calculated enthalpies preclude meaningful comparisons between the different isomers for each framework, although these highly exothermic adsorption enthalpies are consistent with the steep adsorption isotherms and likely arise from a combination of multiple framework−guest interactions.

Qualitative multicomponent vapor-phase breakthrough measurements were performed on Co_2(dobdc) and Co_2(*m*-dobdc) to evaluate their performance in separating an actual mixture of the four C_8 alkylaromatics. In these experiments, N_2 was bubbled through a mixture of *o*-xylene, *m*-xylene, *p*-xylene, and ethylbenzene to produce an equimolar vapor mixture that was subsequently flowed through approximately 1 g of each material at 125 °C. The components of the eluent from the sample columns were determined via gas chromatography and plotted as a function of normalized time (Figure 2c). Consistent with the order of adsorption strengths determined from the single-component adsorption isotherms, *p*-xylene breaks through the Co_2(dobdc) column first followed by *m*-xylene, ethylbenzene, and finally *o*-xylene. In contrast, as was also predicted from the single-component adsorption isotherms, the breakthrough profile of Co_2(*m*-dobdc) shows the elution of *p*-xylene first, followed by *m*-xylene and ethylbenzene simultaneously, and finally *o*-xylene (Figure 2d). Overall, these experiments establish that a four-component mixture of the C_8 isomers can be partitioned in Co_2(dobdc), whereas Co_2(*m*-dobdc) can separate all isomers except ethylbenzene and *m*-xylene.

Although the breakthrough measurements clearly demonstrate separation of the four C_8 isomers in Co_2(dobdc), this experiment was conducted under adsorbate concentrations (∼9−13 mbar partial pressure for each isomer) that are much lower than those typically employed in current adsorption-based processes, which operate in the liquid phase.[4] As the selectivity of an adsorbent can show strong dependence on feed concentration,[21] Co_2(dobdc) was further evaluated through liquid-phase batch adsorption experiments at 33 °C using equimolar solutions of the four isomers (0.040−6.8 M total concentration) in *n*-heptane. The results of these measurements confirm that Co_2(dobdc) maintains its separation performance over a wide range of concentrations (Figure 3 and Figure S22), even when approaching the concentrations in a pure xylenes mixture (∼8 M total concentration). The selectivities calculated from these liquid-phase adsorption experiments (Table 2) agree well with the trends observed in both the single-component vapor-phase adsorption experiments and the multicomponent breakthrough experiments. At the highest total concentration (6.8 M; 1.7 M in each isomer), Co_2(dobdc) is most selective for *o*-xylene over *p*-xylene (3.9 ± 0.5) and least selective for *o*-xylene over ethylbenzene (1.21 ± 0.02). Comparable values have been reported for two-component mixtures of *o*-xylene, *m*-xylene, and *p*-xylene in Ni_2(dobdc), although the reported capacities are much lower.[26]

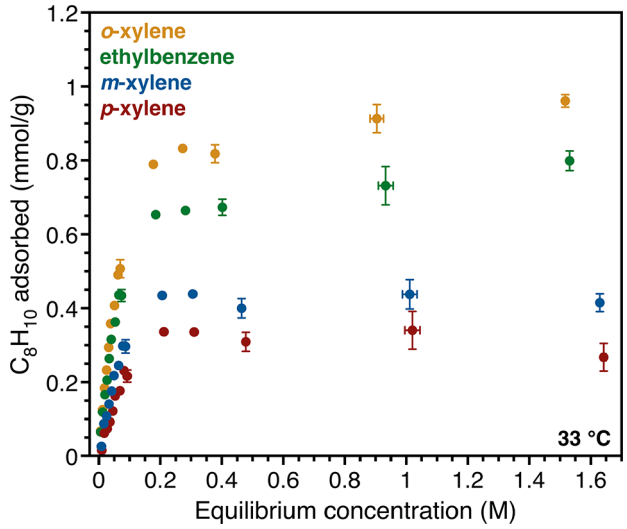

Figure 3. Multicomponent liquid-phase *o*-xylene (yellow), ethylbenzene (green), *m*-xylene (blue), and *p*-xylene (red) adsorption measurements for Co_2(dobdc) at 33 °C using equimolar solutions of the four isomers in *n*-heptane. Data points with error bars (for measurements with initial C_8 isomer concentrations of 0.010, 0.050, 0.10, 0.50, 1.0, and 1.7 M) were determined from an average of three replications. The error bars for data points obtained from measurements with an initial concentration of 0.010 M are smaller than the markers.

Table 2. C_8 Isomer Selectivities for Co_2(dobdc)[a]

C_8 isomers	selectivity
o-xylene/*m*-xylene	2.5 ± 0.1
o-xylene/*p*-xylene	3.9 ± 0.5
o-xylene/ethylbenzene	1.21 ± 0.02
ethylbenzene/*m*-xylene	2.05 ± 0.05
ethylbenzene/*p*-xylene	3.21 ± 0.4
m-xylene/*p*-xylene	1.6 ± 0.2

[a]Determined from a multicomponent liquid-phase adsorption experiment with equimolar amounts of the C_8 isomers (1.7 M in each isomer; 6.8 M total concentration) in *n*-heptane at 33 °C.

The foregoing data suggest that Co_2(dobdc) could facilitate the separation of all four C_8 isomers in a single industrial

DOI: 10.1021/jacs.7b13825
J. Am. Chem. Soc. 2018, 140, 3412−3422

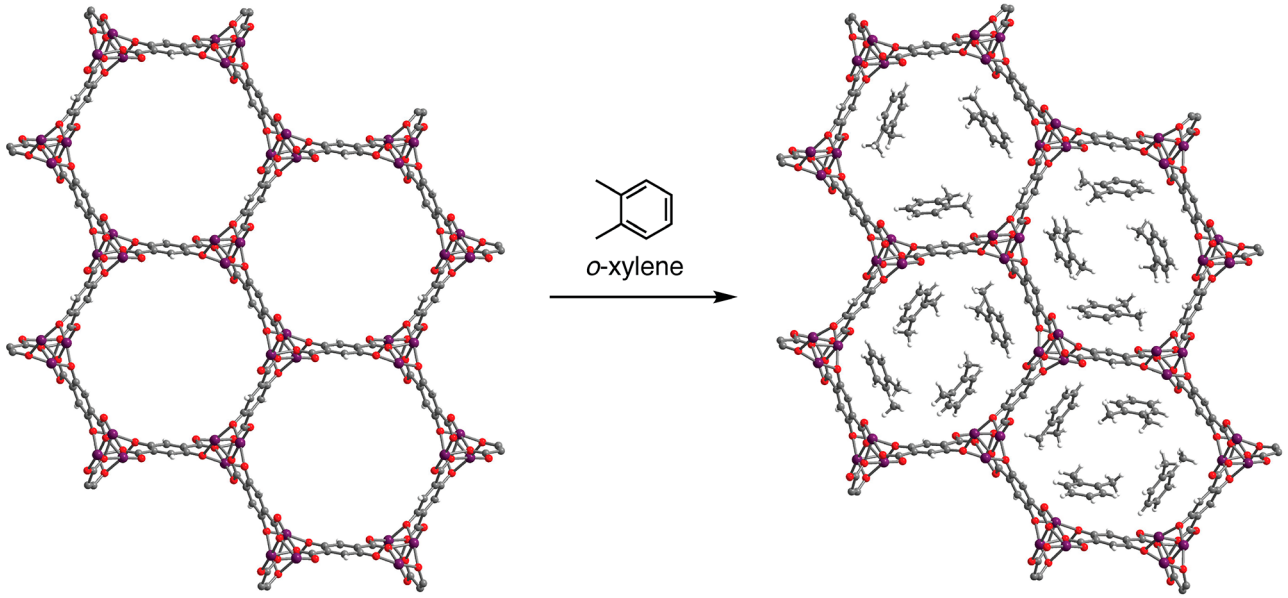

Figure 4. Structural distortion of Co_2(dobdc) upon adsorption of *o*-xylene as determined by single-crystal X-ray diffraction at 100 K. Three out of four channels distort to accommodate an additional equivalent of *o*-xylene. The *o*-xylene molecules in the undistorted pore were found to be disordered over two sets of locations due to the $\bar{3}$ symmetry of the framework, but only one set is shown here for clarity. Purple, red, gray, and white spheres represent Co, O, C, and H atoms, respectively.

adsorption process, which would be especially useful for removing ethylbenzene from C_8 mixtures. Although unable to separate all four isomers, Co_2(*m*-dobdc) could conceivably be applicable in current xylenes separation processes, wherein the *p*-xylene and *o*-xylene are obtained by separation and the mixture of *m*-xylene and ethylbenzene is regioisomerized to the equilibrium mixture. In addition, Co_2(*m*-dobdc) and its isostructural analogues with other metal cations also offer the advantage of combining high adsorption performance with low materials' cost as compared to that of other metal−organic frameworks.[54] The selectivity of both cobalt frameworks for the other isomers over *p*-xylene could even be used in the separation of these components from the 90+% *p*-xylene product mixtures of toluene disproportionation processes.[55]

Structural Characterization of C_8 Isomer Adsorption. Single-crystal X-ray diffraction studies were performed to elucidate the structural features that underlie the ability of these frameworks to bind and differentiate the C_8 isomers. In general, structures were obtained from data collected at 100 K on single crystals that were soaked for ∼24 h in an aliquot of each C_8 alkylaromatic. Contrary to the structural rigidity maintained by the M_2(dobdc) series of metal−organic frameworks upon adsorption of different small molecules,[32−35,38,56−70] Co_2(dobdc) exhibits appreciable flexibility upon adsorption of the two strongest binding isomers, *o*-xylene and ethylbenzene. Upon binding either of these isomers, three out of every four pores in the framework elongate along the direction perpendicular to two opposing edges of the hexagonal channel (Figure 4). The arrangement of six deformed channels around a single undistorted channel maintains the $R\bar{3}$ symmetry of the lattice but lowers its translational symmetry, which manifests in the formation of a supercell with *a* and *b* edges that are double that of the undistorted framework. Notably, these experimental results corroborate computational work predicting similar adsorbate-induced lattice distortions in expanded variants of this framework.[71]

Remarkably, each distorted pore in the *o*-xylene structure accommodates four xylene molecules for every three adsorbed in an undistorted channel, resulting in three distinct binding sites for *o*-xylene in the framework (Figure 4 and Figure S3). Two cobalt(II) centers interact with a single *o*-xylene molecule at two of these sites, one located in a deformed channel and the other in an undistorted channel. In the third site, *o*-xylene binds to only a single cobalt(II) center through η^2 coordination of the aromatic ring. Only one binding site was resolved in the structure of ethylbenzene in Co_2(dobdc), which is located in the distorted pore of the framework (Figure S5). In contrast, no framework distortion occurs when *m*-xylene or *p*-xylene bind to Co_2(dobdc), and for these isomers only one xylene molecule is adsorbed for every two cobalt sites at full occupancy (Figures S1 and S2), consistent with the saturation capacities measured from the single-component adsorption isotherms.

In the *o*-xylene and ethylbenzene structures, the two cobalt centers interacting with a single molecule in the distorted channels are brought ∼0.2 Å closer together than in the activated framework (7.854(2) Å with *o*-xylene and 7.897(3) Å with ethylbenzene as compared to 8.0771(12) Å in the activated framework). This contraction facilitates a closer contact between the exposed cobalt sites and the adsorbate, resulting in greater stabilization of the adsorbed *o*-xylene or ethylbenzene molecules. As the framework distortion only occurs upon adsorption of the two strongest binding isomers, we can infer that this structural change requires sufficiently strong framework−guest interactions, while the tight packing of *o*-xylene molecules in the deformed channels suggests that guest−guest interactions also play a key role. Altogether, these structural results indicate that distortion of the framework is governed by an interplay between the energetic penalty incurred upon framework deformation and the thermodynamic stability gained through enhanced framework−guest interactions and the adsorption of additional molecules upon distortion.

DOI: 10.1021/jacs.7b13825
J. Am. Chem. Soc. 2018, 140, 3412−3422

To determine whether the structural distortion of Co_2(dobdc) occurs at temperatures relevant to those employed in evaluating C_8 isomer separations, we carried out variable-temperature powder X-ray diffraction studies on *o*-xylene- and ethylbenzene-soaked samples of the framework from 27−127 °C (Figures S23 and S24). These experiments revealed that the distortion only happens at temperatures well below those of the single-component adsorption isotherms (150 °C) and breakthrough measurements (125 °C). Specifically, *o*-xylene induces framework distortion at temperatures lower than or equal to 67 °C, while the ethylbenzene-soaked sample remained undistorted even as low as 27 °C. Moreover, diffraction experiments at 100 K on single crystals taken from the multicomponent liquid-phase batch adsorption measurements showed no evidence of the distortion, indicating that the presence of the other isomers prevents *o*-xylene and ethylbenzene from distorting the framework. Thus, the observed separation performance of Co_2(dobdc) under the conditions of the breakthrough and liquid-phase adsorption experiments cannot be attributed to the flexibility of the framework. Comparing the *o*-xylene adsorption isotherms at 50 and 150 °C, however, demonstrates the distortion does impact the adsorption properties of the framework. Indeed, the saturation capacity at 150 °C corresponds to the loading of one *o*-xylene per two cobalt sites in the undistorted pore (3.2 mmol *o*-xylene), whereas the isotherm at 50 °C displays the anticipated 25% increase in capacity that accompanies the distortion (Figure 5).

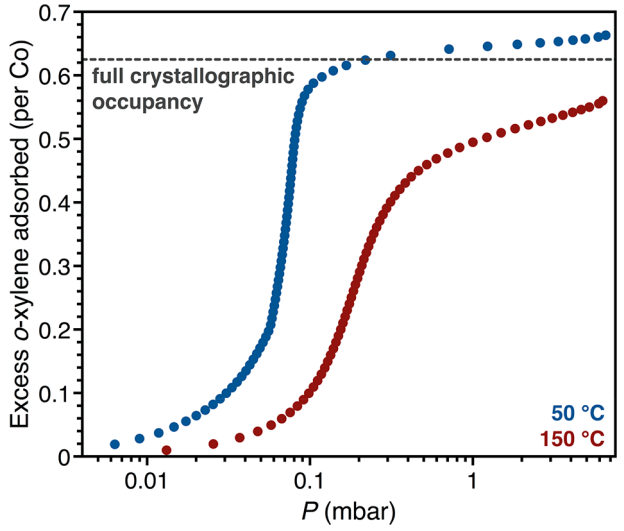

Figure 5. Comparison of the *o*-xylene adsorption isotherms for Co_2(dobdc) at 50 °C (blue) and 150 °C (red). The saturation capacity at 50 °C corresponds well with full crystallographic occupancy of all of he *o*-xylene sites in the structure of *o*-xylene in Co_2(dobdc) at 100 K, whereas the capacity at 150 °C matches a loading of one *o*-xylene per two cobalt sites in an undistorted pore.

Comparison of the structures of the four isomers in Co_2(dobdc) at 100 K reveals that each isomer interacts with both the exposed cobalt(II) sites and the linker aromatic rings (Figure 6). All four isomers display comparable arene $\pi-\pi$ interactions with the dobdc^{4-} linker, with centroid-to-centroid distances that range from 3.583(4) Å for *p*-xylene to 3.651(9) Å for *o*-xylene. The similarity of these distances and lack of an apparent trend with binding affinity suggest that $\pi-\pi$ interactions do not contribute significantly to the xylene isomer selectivity. In contrast, clear differences can be identified in the interactions of each isomer with the exposed cobalt(II) sites of the framework. Significantly, *o*-xylene, ethylbenzene, and *m*-xylene are capable of interacting with two cobalt(II) centers situated at opposite ends of a linker, whereas *p*-xylene, the weakest binding isomer, interacts with only a single metal site. Two of the binding sites for *o*-xylene feature the interaction of a methyl group and an aryl C−H group at the 1 and 4 positions of the *o*-xylene ring with two cobalt(II) centers on opposing sides of a dobdc^{4-} linker (Figure 6 and Figure S4), with Co···C_{methyl} distances of 3.101(19) and 3.13(5) Å and Co···C_{aryl} distances of 2.789(19) and 2.9130(18) Å, respectively. These distances are much longer than those observed for agostic interaction in alkyl and aryl complexes,[72−78] indicating that the xylene molecule binds through weak noncovalent interactions that arise from polarization by the exposed partial positive charge on the cobalt centers. We note that, although another binding mode was identified for *o*-xylene in the distorted structure of Co_2(dobdc) (Figure S4), this site is less relevant as the distortion does not occur under the conditions of the multicomponent separation.

Ethylbenzene also interacts with two metal sites through a benzylic carbon and an opposing aryl C−H group. Both interactions are longer than those observed with *o*-xylene, in line with the lower affinity of Co_2(dobdc) for ethylbenzene (Figure 6). These comparatively weaker Co^{II}−ethylbenzene interactions likely result from the additional steric bulk of the ethyl group, which prevents a closer approach of molecule to the cobalt sites and is evident in the much longer Co···C_{benzyl} distance (3.35(3) Å) of ethylbenzene as compared to the Co···C_{methyl} distance of *o*-xylene (3.101(19) Å).

The second weakest adsorbing isomer, *m*-xylene, also binds to two cobalt(II) sites through opposing alkyl and aryl C−H groups. In comparison to *o*-xylene and ethylbenzene, *m*-xylene exhibits a longer Co···C_{aryl} distance of 3.0164(3) Å, which can be attributed to steric repulsion between the adjacent methyl group and a linker oxygen atom that is only 3.34(3) Å away. The longer Co···C_{aryl} distance suggests that a weaker Co^{II}−aryl interaction leads to the lower affinity of the framework for this isomer.

The 1,4 substitution of *p*-xylene causes it to be too long to adopt the same orientation as the other C_8 isomers, precluding its interaction with two metal sites. As a consequence, this isomer is only stabilized by the interaction of an aryl C−H group with a single cobalt(II) center and an arene $\pi-\pi$ interaction with the linker. The absence of a second Co^{II}−*p*-xylene interaction results in this isomer binding the weakest to Co_2(dobdc). Single-component adsorption isotherms from an expanded analogue of this material, Co_2(dobpdc) (dobpdc^{4-} = 4,4′-dioxidobiphenyl-3,3′-dicarboxylate),[42] corroborate that interaction with only a single metal site leads to weaker adsorption of the C_8 isomers, as the longer distances between the two cobalt(II) centers across each linker in this material prevent any of the four isomers from interacting with both cobalt sites (Figure S21).

Interestingly, Co_2(*m*-dobdc) does not exhibit pore distortion upon binding any of the isomers at the investigated temperatures. The lack of any observed distortion likely arises from the closer distance between the cobalt(II) centers in Co_2(*m*-dobdc) (7.7923(15) Å) as compared to Co_2(dobdc) (8.0771(12) Å). This difference of ∼0.2 Å matches well with the observed change in Co···Co distance upon framework distortion in Co_2(dobdc) and likely precludes the need for a

DOI: 10.1021/jacs.7b13825
J. Am. Chem. Soc. 2018, 140, 3412−3422

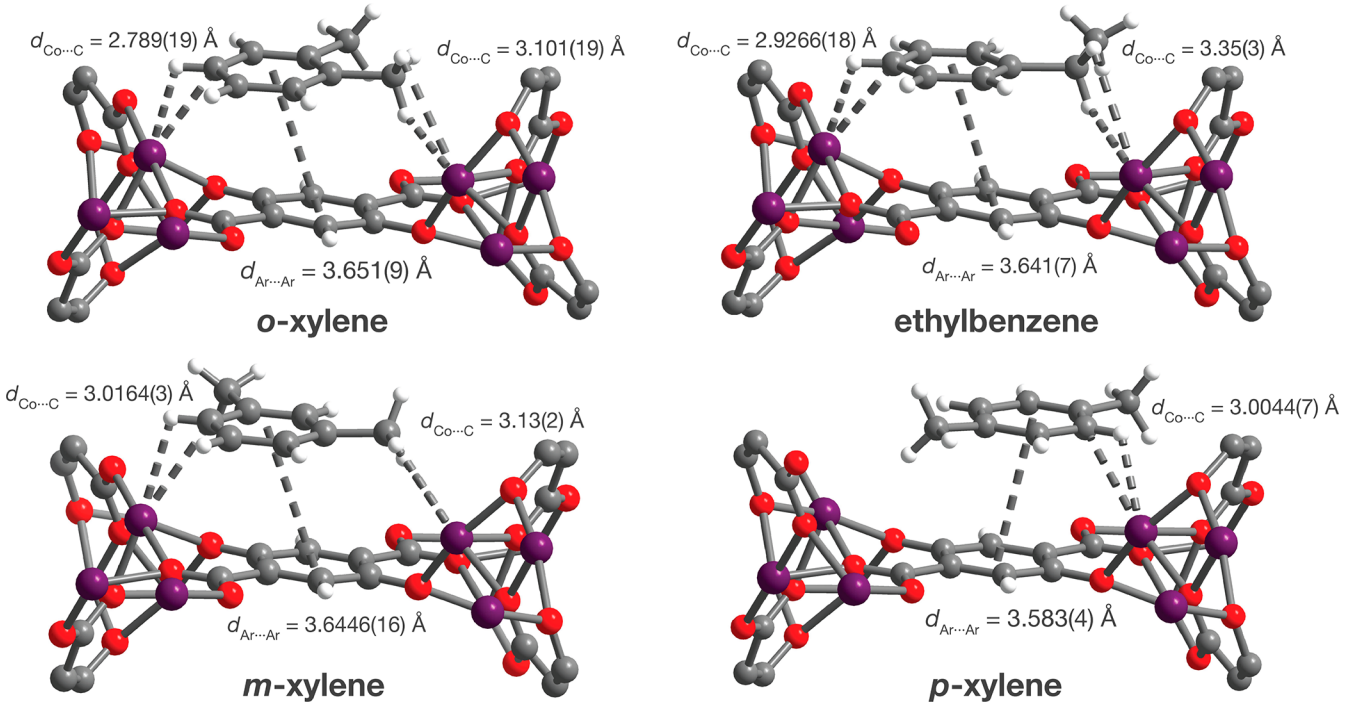

Figure 6. A portion of the structures of *o*-xylene, ethylbenzene, *m*-xylene, and *p*-xylene in Co_2(dobdc) at 100 K as determined through analysis of single-crystal X-ray diffraction data, showing the interactions of each isomer with two exposed cobalt(II) sites and the linker arene ring. The structures shown for *o*-xylene and ethylbenzene correspond to binding sites within the distorted hexagonal channels. Two additional binding sites were located for *o*-xylene (Figure S4). Purple, red, gray, and white spheres represent Co, O, C, and H atoms, respectively.

distortion to maximize the interaction between two metal sites and a single C_8 molecule in Co_2(*m*-dobdc). Furthermore, this difference in behavior between the isomeric frameworks highlights how subtle changes in the framework structure can affect its adsorption properties. As in Co_2(dobdc), *o*-xylene and ethylbenzene were also observed to bind to two cobalt(II) sites in Co_2(*m*-dobdc) through the interaction of an alkyl group and an aryl C−H group (Figure 7), resulting in three binding sites in each hexagonal channel related by 3-fold symmetry (Figures S6 and S7). The stronger binding isomer, *o*-xylene, displays a shorter Co···C_{aryl} distance of 2.7954(7) Å and a similar Co···C_{alkyl} distance of 2.89(3) Å as compared to the respective distances of 3.09(3) and 2.81(4) Å for ethylbenzene, suggesting that Co_2(*m*-dobdc) also distinguishes between the two isomers through the strength of their interactions with two metal sites. Although sufficiently resolved structures of the other C_8 alkylaromatic molecules in Co_2(*m*-dobdc) could not be obtained due to severe disorder enforced by the mirror symmetry of the framework, the selectivity of Co_2(*m*-dobdc) for the different isomers is expected to be controlled by factors similar to those identified in Co_2(dobdc).

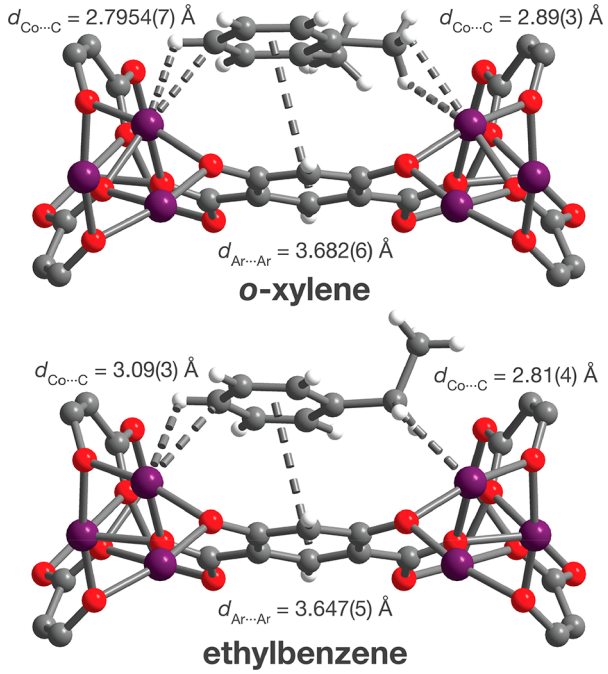

Figure 7. A portion of the structures of *o*-xylene and ethylbenzene in Co_2(*m*-dobdc) at 100 K as determined through analysis of single-crystal X-ray diffraction data, showing the interactions of each isomer with two exposed cobalt(II) sites and the linker arene ring. The C_8 isomers in both structures are disordered over two positions due to the mirror symmetry of the framework. Water was found to contaminate 30% of the cobalt(II) sites in the structure of ethylbenzene in Co_2(*m*-dobdc), but only ethylbenzene is shown here for clarity. Purple, red, gray, and white spheres represent Co, O, C, and H atoms, respectively.

CONCLUSIONS

The foregoing results demonstrate that the C_8 alkylaromatics *o*-xylene, *m*-xylene, *p*-xylene, and ethylbenzene can be separated by the metal−organic frameworks Co_2(dobdc) and Co_2(*m*-dobdc) through the varied extent of interaction of each isomer with two adjacent coordinatively unsaturated cobalt(II) centers. Single-component adsorption isotherms, multicomponent vapor-phase breakthrough measurements, and multicomponent liquid-phase batch adsorption experiments show that Co_2(dobdc) effectively separates all four isomers and has the strongest affinity for *o*-xylene, followed by ethylbenzene, *m*-

DOI: 10.1021/jacs.7b13825
J. Am. Chem. Soc. 2018, 140, 3412−3422

xylene, and *p*-xylene. In contrast, Co_2(*m*-dobdc) can only distinguish between three of the four isomers, due to its similar binding affinity for *m*-xylene and ethylbenzene.

Single-crystal X-ray diffraction experiments indicate that the strong adsorption of the C_8 alkylaromatics arises from their interactions with a linker aromatic ring and exposed cobalt(II) sites in both Co_2(dobdc) and Co_2(*m*-dobdc). In particular, a comparison of the structures of the four xylene isomers in Co_2(dobdc) shows that the framework distinguishes among the isomers due to nuanced differences in the interaction of *o*-xylene, ethylbenzene, and *m*-xylene with two adjacent cobalt(II) centers and the inability of *p*-xylene to interact with a second metal site. Furthermore, the structures of *o*-xylene and ethylbenzene in Co_2(dobdc) reveal that the framework undergoes an unprecedented structural distortion upon binding of these isomers, allowing the accommodation of additional adsorbate molecules.

Altogether, these results highlight how leveraging the interaction of multiple coordinatively unsaturated metal centers with a single molecule may lead to the design of new adsorbents for the separation of hydrocarbons. In particular, altering the distance between the exposed metal sites in related materials could afford control over their selectivity for the different C_8 isomers and could potentially enable the separation of mixtures containing other adsorbates.

■ ASSOCIATED CONTENT

Supporting Information

The Supporting Information is available free of charge on the ACS Publications website at DOI: 10.1021/jacs.7b13825.

X-ray crystallographic data for Co_2(dobdc)·0.99(*o*-xylene) (CIF)

X-ray crystallographic data for Co_2(dobdc)·0.36(ethylbenzene) (CIF)

X-ray crystallographic data for Co_2(dobdc)·0.74(*m*-xylene) (CIF)

X-ray crystallographic data for Co_2(dobdc)·0.82(*p*-xylene) (CIF)

X-ray crystallographic data for Co_2(*m*-dobdc)·0.92(*o*-xylene) (CIF)

X-ray crystallographic data for Co_2(*m*-dobdc)$(H_2O)_{0.61}$·0.77(ethylbenzene) (CIF)

Additional experimental details, supplementary figures, crystallographic information, single-component adsorption isotherm data, and powder X-ray diffraction data (PDF)

■ AUTHOR INFORMATION

Corresponding Author

*jrlong@berkeley.edu

ORCID

Eric D. Bloch: 0000-0003-4507-6247

Jeffrey R. Long: 0000-0002-5324-1321

Present Addresses

[#]University of Delaware, Newark, Delaware 19716, United States.

[▽]Harvard University, Cambridge, Massachusetts 02138, United States.

Author Contributions

[○]M.I.G. and M.T.K. contributed equally.

Notes

The authors declare the following competing financial interest(s): The University of California, Berkeley has applied for a patent on some of the technology discussed herein, on which J.R.L, E.D.B., M.T.K, and M.I.G. are inventors. J.R.L. has a financial interest in Mosaic Materials, Inc., a startup company working to commercialize metal−organic frameworks, including M_2(*m*-dobdc).

■ ACKNOWLEDGMENTS

This work was supported through the Center for Gas Separations Relevant to Clean Energy Technologies, an Energy Frontier Research Center funded by the U.S. Department of Energy, Office of Science, Office of Basic Energy Sciences under award DE-SC0001015. This research used resources of the Advanced Light Source, which is supported by the Director, Office of Science, Office of Basic Energy Sciences, of the U.S. Department of Energy under contract no. DE-AC02-05CH11231, and the Advanced Photon Source, a DoE Office of Science User Facility operated by Argonne National Laboratory under contract no. DE-AC02-06CH11357. We thank Greg Halder and the 17-BM-B staff for experimental assistance. M.T.K. and D.A.R. thank the National Science Foundation for graduate fellowship support. P.J.M. thanks the National Institute of General Medical Sciences of the National Institutes of Health for a postdoctoral fellowship (F32GM120799). G.B. thanks the Miller Institute for Basic Research in Science for a postdoctoral fellowship. We acknowledge Katie R. Meihaus for editorial assistance. We also thank Simon J. Teat and Rebecca L. Siegelman for helpful discussions.

■ REFERENCES

(1) Sholl, D. S.; Lively, R. P. *Nature* **2016**, *532*, 435−437.

(2) Fabri, J.; Graeser, U.; Simo, T. A. *Ullman's Encyclopedia of Industrial Chemistry*; Wiley-VCH Verlag GmbH & Co. KGaA: New York, 2000.

(3) Denayer, J. F. M.; De Vos, D.; Leflaive, P. In *Metal-Organic Frameworks*; Farrusseng, D., Ed.; Applications from Catalysis to Gas Storage; Wiley-VCH Verlag GmbH & Co. KGaA: Weinheim, Germany, 2011; Vol. *83*, pp 171−190.

(4) Minceva, M.; Rodrigues, A. E. *AIChE J.* **2007**, *53*, 138−149.

(5) Pellegrino, J. L. *Energy and Environmental Profile of the Chemicals Industry*; U.S. Department of Energy, 2000.

(6) Welch, V. A.; Fallon, K. J.; Gelbke, H.-P. *Ethylbenzene*; Wiley-VCH Verlag GmbH & Co. KGaA: Weinheim, Germany, 2000; Vol. *13*, pp 451−414.

(7) Li, J.-R.; Kuppler, R. J.; Zhou, H.-C. *Chem. Soc. Rev.* **2009**, *38* (5), 1477−29.

(8) Guo, G.-Q.; Chen, H.; Long, Y.-C. *Microporous Mesoporous Mater.* **2000**, *39*, 149−161.

(9) Yang, Y.; Bai, P.; Guo, X. *Ind. Eng. Chem. Res.* **2017**, *56*, 14725−14753.

(10) Hulme, R.; Rosensweig, R. E.; Ruthven, D. M. *Ind. Eng. Chem. Res.* **1991**, *30*, 752−760.

(11) Yan, T. Y. *Ind. Eng. Chem. Res.* **1989**, *28*, 572−576.

(12) Ruthven, D. M.; Goddard, M. *Zeolites* **1986**, *6*, 275−282.

(13) Santacesaria, E.; Morbidelli, M.; Servida, A.; Storti, G.; Carra, S. *Ind. Eng. Chem. Process Des. Dev.* **1982**, *21*, 446−451.

(14) Koh, D.-Y.; McCool, B. A.; Deckman, H. W.; Lively, R. P. *Science* **2016**, *353*, 804−807.

(15) Herm, Z. R.; Bloch, E. D.; Long, J. R. *Chem. Mater.* **2014**, *26*, 323−338.

(16) Peralta, D.; Chaplais, G.; Paillaud, J.-L.; Simon-Masseron, A.; Barthelet, K.; Pirngruber, G. D. *Microporous Mesoporous Mater.* **2013**, *173*, 1−5.

DOI: 10.1021/jacs.7b13825
J. Am. Chem. Soc. 2018, 140, 3412−3422

(17) Huang, W.; Jiang, J.; Wu, D.; Xu, J.; Xue, B.; Kirillov, A. M. *Inorg. Chem.* **2015**, *54*, 10524−10526.
(18) Van de Voorde, B.; Bueken, B.; Denayer, J.; De Vos, D. *Chem. Soc. Rev.* **2014**, *43*, 5766−5788.
(19) Alaerts, L.; Kirschhock, C. E. A.; Maes, M.; van der Veen, M. A.; Finsy, V.; Depla, A.; Martens, J. A.; Baron, G. V.; Jacobs, P. A.; Denayer, J. F. M.; De Vos, D. E. *Angew. Chem., Int. Ed.* **2007**, *46*, 4293−4297.
(20) Alaerts, L.; Maes, M.; Jacobs, P. A.; Denayer, J. F. M.; De Vos, D. E. *Phys. Chem. Chem. Phys.* **2008**, *10*, 2979−2985.
(21) Finsy, V.; Verelst, H.; Alaerts, L.; De Vos, D.; Jacobs, P. A.; Baron, G. V.; Denayer, J. F. M. *J. Am. Chem. Soc.* **2008**, *130*, 7110−7118.
(22) Alaerts, L.; Maes, M.; Giebeler, L.; Jacobs, P. A.; Martens, J. A.; Denayer, J. F. M.; Kirschhock, C. E. A.; De Vos, D. E. *J. Am. Chem. Soc.* **2008**, *130*, 14170−14178.
(23) Gu, Z.-Y.; Jiang, D.-Q.; Wang, H.-F.; Cui, X.-Y.; Yan, X.-P. *J. Phys. Chem. C* **2010**, *114*, 311−316.
(24) Bárcia, P. S.; Guimarães, D.; Mendes, P. A. P.; Silva, J. A. C.; Guillerm, V.; Chevreau, H.; Serre, C.; Rodrigues, A. E. *Microporous Mesoporous Mater.* **2011**, *139*, 67−73.
(25) Vermoortele, F.; Maes, M.; Moghadam, P. Z.; Lennox, M. J.; Ragon, F.; Boulhout, M.; Biswas, S.; Laurier, K. G. M.; Beurroies, I.; Denoyel, R.; Roeffaers, M.; Stock, N.; Düren, T.; Serre, C.; De Vos, D. E. *J. Am. Chem. Soc.* **2011**, *133*, 18526−18529.
(26) Peralta, D.; Barthelet, K.; Pérez-Pellitero, J.; Chizallet, C.; Chaplais, G.; Simon-Masseron, A.; Pirngruber, G. D. *J. Phys. Chem. C* **2012**, *116*, 21844−21855.
(27) Warren, J. E.; Perkins, C. G.; Jelfs, K. E.; Boldrin, P.; Chater, P. A.; Miller, G. J.; Manning, T. D.; Briggs, M. E.; Stylianou, K. C.; Claridge, J. B.; Rosseinsky, M. J. *Angew. Chem., Int. Ed.* **2014**, *53*, 4592−4596.
(28) Osta El, R.; Carlin-Sinclair, A.; Guillou, N.; Walton, R. I.; Vermoortele, F.; Maes, M.; De Vos, D.; Millange, F. *Chem. Mater.* **2012**, *24*, 2781−2791.
(29) Agrawal, M.; Bhattacharyya, S.; Huang, Y.; Jayachandrababu, K. C.; Murdock, C. R.; Bentley, J. A.; Rivas-Cardona, A.; Mertens, M. M.; Walton, K. S.; Sholl, D. S.; Nair, S. *J. Phys. Chem. C* **2018**, *122*, 386−397.
(30) Caskey, S. R.; Wong-Foy, A. G.; Matzger, A. J. *J. Am. Chem. Soc.* **2008**, *130*, 10870−10871.
(31) Dietzel, P. D. C.; Besikiotis, V.; Blom, R. *J. Mater. Chem.* **2009**, *19*, 7362−7370.
(32) Bloch, E. D.; Murray, L. J.; Queen, W. L.; Chavan, S.; Maximoff, S. N.; Bigi, J. P.; Krishna, R.; Peterson, V. K.; Grandjean, F.; Long, G. J.; Smit, B.; Bordiga, S.; Brown, C. M.; Long, J. R. *J. Am. Chem. Soc.* **2011**, *133*, 14814−14822.
(33) Bloch, E. D.; Queen, W. L.; Krishna, R.; Zadrozny, J. M.; Brown, C. M.; Long, J. R. *Science* **2012**, *335*, 1606−1610.
(34) Bloch, E. D.; Hudson, M. R.; Mason, J. A.; Chavan, S.; Crocellà, V.; Howe, J. D.; Lee, K.; Dzubak, A. L.; Queen, W. L.; Zadrozny, J. M.; Geier, S. J.; Lin, L.-C.; Gagliardi, L.; Smit, B.; Neaton, J. B.; Bordiga, S.; Brown, C. M.; Long, J. R. *J. Am. Chem. Soc.* **2014**, *136*, 10752−10761.
(35) Queen, W. L.; Hudson, M. R.; Bloch, E. D.; Mason, J. A.; Gonzalez, M. I.; Lee, J. S.; Gygi, D.; Howe, J. D.; Lee, K.; Darwish, T. A.; James, M.; Peterson, V. K.; Teat, S. J.; Smit, B.; Neaton, J. B.; Long, J. R.; Brown, C. M. *Chem. Sci.* **2014**, *5*, 4569−4581.
(36) Xiao, D. J.; Gonzalez, M. I.; Darago, L. E.; Vogiatzis, K. D.; Haldoupis, E.; Gagliardi, L.; Long, J. R. *J. Am. Chem. Soc.* **2016**, *138*, 7161−7170.
(37) Reed, D. A.; Xiao, D. J.; Gonzalez, M. I.; Darago, L. E.; Herm, Z. R.; Grandjean, F.; Long, J. R. *J. Am. Chem. Soc.* **2016**, *138*, 5594−5602.
(38) Geier, S. J.; Mason, J. A.; Bloch, E. D.; Queen, W. L.; Hudson, M. R.; Brown, C. M.; Long, J. R. *Chem. Sci.* **2013**, *4*, 2054−2061.
(39) Bloch, E. D.; Queen, W. L.; Hudson, M. R.; Mason, J. A.; Xiao, D. J.; Murray, L. J.; Flacau, R.; Brown, C. M.; Long, J. R. *Angew. Chem.* **2016**, *128*, 8747−8751.
(40) Murray, L. J.; Dincă, M.; Yano, J.; Chavan, S.; Bordiga, S.; Brown, C. M.; Long, J. R. *J. Am. Chem. Soc.* **2010**, *132*, 7856−7857.
(41) Sumida, K.; Rogow, D. L.; Mason, J. A.; McDonald, T. M.; Bloch, E. D.; Herm, Z. R.; Bae, T.-H.; Long, J. R. *Chem. Rev.* **2012**, *112*, 724−781.
(42) Gygi, D.; Bloch, E. D.; Mason, J. A.; Hudson, M. R.; Gonzalez, M. I.; Siegelman, R. L.; Darwish, T. A.; Queen, W. L.; Brown, C. M.; Long, J. R. *Chem. Mater.* **2016**, *28*, 1128−1138.
(43) Dietzel, P. D. C.; Morita, Y.; Blom, R.; Fjellvåg, H. *Angew. Chem., Int. Ed.* **2005**, *44*, 6354−6358.
(44) Kapelewski, M. T.; Geier, S. J.; Hudson, M. R.; Stück, D.; Mason, J. A.; Nelson, J. N.; Xiao, D. J.; Hulvey, Z.; Gilmour, E.; FitzGerald, S. A.; Head-Gordon, M.; Brown, C. M.; Long, J. R. *J. Am. Chem. Soc.* **2014**, *136*, 12119−12129.
(45) Bruker Analytical X-ray Systems, Inc. *SAINT and APEX 2 Software for CCD Diffractometers*; Bruker Analytical X-ray Systems, Inc.: Madison, WI, 2000.
(46) Sheldrick, G. M. *SADABS*; Bruker Analytical X-ray Systems, Inc.: Madison, WI, 2014.
(47) Sheldrick, G. M. *Acta Crystallogr., Sect. A: Found. Crystallogr.* **2008**, *64*, 112−122.
(48) Sheldrick, G. M. *SHELXS*; University of Göttingen: Germany, 2014.
(49) Sheldrick, G. M. *Acta Crystallogr., Sect. A: Found. Adv.* **2015**, *71*, 3−8.
(50) Sheldrick, G. M. *SHELXL*; University of Göttingen: Germany, 2014.
(51) Dolomanov, O. V.; Bourhis, L. J.; Gildea, R. J.; Howard, J. A. K.; Puschmann, H. *J. Appl. Crystallogr.* **2009**, *42*, 339−341.
(52) Minceva, M.; Rodrigues, A. E. *Chem. Eng. Res. Des.* **2004**, *82*, 667−681.
(53) Bellat, J.-P.; Simonot-Grange, M.-H.; Jullian, S. *Zeolites* **1995**, *15*, 124−130.
(54) DeSantis, D.; Mason, J. A.; James, B. D.; Houchins, C.; Long, J. R.; Veenstra, M. *Energy Fuels* **2017**, *31*, 2024−2032.
(55) Perego, C.; Pollesel, P. In *Advances in Nanoporous Materials*; Ernst, S., Ed.; Advances in Nanoporous Materials; Elsevier: New York, 2010; Vol. *1*, pp 97−149.
(56) Dietzel, P. D. C.; Georgiev, P. A.; Eckert, J.; Blom, R.; Strässle, T.; Unruh, T. *Chem. Commun.* **2010**, *46*, 4962−4963.
(57) Xiao, D. J.; Bloch, E. D.; Mason, J. A.; Queen, W. L.; Hudson, M. R.; Planas, N.; Borycz, J.; Dzubak, A. L.; Verma, P.; Lee, K.; Bonino, F.; Crocellà, V.; Yano, J.; Bordiga, S.; Truhlar, D. G.; Gagliardi, L.; Brown, C. M.; Long, J. R. *Nat. Chem.* **2014**, *6*, 590−595.
(58) McKinlay, A. C.; Xiao, B.; Wragg, D. S.; Wheatley, P. S.; Megson, I. L.; Morris, R. E. *J. Am. Chem. Soc.* **2008**, *130*, 10440−10444.
(59) Bloch, E. D.; Queen, W. L.; Chavan, S.; Wheatley, P. S.; Zadrozny, J. M.; Morris, R.; Brown, C. M.; Lamberti, C.; Bordiga, S.; Long, J. R. *J. Am. Chem. Soc.* **2015**, *137*, 3466−3469.
(60) Sumida, K.; Her, J.-H.; Dincă, M.; Murray, L. J.; Schloss, J. M.; Pierce, C. J.; Thompson, B. A.; FitzGerald, S. A.; Brown, C. M.; Long, J. R. *J. Phys. Chem. C* **2011**, *115*, 8414−8421.
(61) Queen, W. L.; Bloch, E. D.; Brown, C. M.; Hudson, M. R.; Mason, J. A.; Murray, L. J.; Ramirez-Cuesta, A. J.; Peterson, V. K.; Long, J. R. *Dalton Trans.* **2012**, *41*, 4180−4188.
(62) Lee, J. S.; Vlaisavljevich, B.; Britt, D. K.; Brown, C. M.; Haranczyk, M.; Neaton, J. B.; Smit, B.; Long, J. R.; Queen, W. L. *Adv. Mater.* **2015**, *27*, 5785−5796.
(63) Bloch, W. M.; Burgun, A.; Coghlan, C. J.; Lee, R.; Coote, M. L.; Doonan, C. J.; Sumby, C. J. *Nat. Chem.* **2014**, *6*, 906−912.
(64) Furukawa, H.; Gándara, F.; Zhang, Y.-B.; Jiang, J.; Queen, W. L.; Hudson, M. R.; Yaghi, O. M. *J. Am. Chem. Soc.* **2014**, *136*, 4369−4381.
(65) Magdysyuk, O. V.; Adams, F.; Liermann, H.-P.; Spanopoulos, I.; Trikalitis, P. N.; Hirscher, M.; Morris, R. E.; Duncan, M. J.; McCormick, L. J.; Dinnebier, R. E. *Phys. Chem. Chem. Phys.* **2014**, *16*, 23908−23914.
(66) Ghose, S. K.; Li, Y.; Yakovenko, A.; Dooryhee, E.; Ehm, L.; Ecker, L. E.; Dippel, A.-C.; Halder, G. J.; Strachan, D. M.; Thallapally, P. K. *J. Phys. Chem. Lett.* **2015**, *6*, 1790−1794.

DOI: 10.1021/jacs.7b13825
J. Am. Chem. Soc. 2018, 140, 3412−3422

(67) Dietzel, P. D. C.; Johnsen, R. E.; Fjellvåg, H.; Bordiga, S.; Groppo, E.; Chavan, S.; Blom, R. *Chem. Commun.* **2008**, 5125−5127.
(68) Liu, Y.; Kabbour, H.; Brown, C. M.; Neumann, D. A.; Ahn, C. C. *Langmuir* **2008**, *24*, 4772−4777.
(69) Gonzalez, M. I.; Mason, J. A.; Bloch, E. D.; Teat, S. J.; Gagnon, K. J.; Morrison, G. Y.; Queen, W. L.; Long, J. R. *Chem. Sci.* **2017**, *8*, 4387−4398.
(70) Rosnes, M. H.; Sheptyakov, D.; Franz, A.; Frontzek, M.; Dietzel, P. D. C.; Georgiev, P. A. *Phys. Chem. Chem. Phys.* **2017**, *103*, 2347.
(71) Jawahery, S.; Simon, C. M.; Braun, E.; Witman, M.; Tiana, D.; Vlaisavljevich, B.; Smit, B. *Nat. Commun.* **2016**, *8*, 1−9.
(72) Pike, S. D.; Thompson, A. L.; Algarra, A. G.; Apperley, D. C.; Macgregor, S. A.; Weller, A. S. *Science* **2012**, *337*, 1648−1651.
(73) Pike, S. D.; Chadwick, F. M.; Rees, N. H.; Scott, M. P.; Weller, A. S.; Krämer, T.; Macgregor, S. A. *J. Am. Chem. Soc.* **2015**, *137*, 820−833.
(74) Chadwick, F. M.; Rees, N. H.; Weller, A. S.; Krämer, T.; Iannuzzi, M.; Macgregor, S. A. *Angew. Chem., Int. Ed.* **2016**, *55*, 3677−3681.
(75) Vigalok, A.; Uzan, O.; Shimon, L. J. W.; Ben-David, Y.; Martin, J. M. L.; Milstein, D. *J. Am. Chem. Soc.* **1998**, *120*, 12539−12544.
(76) Dani, P.; Karlen, T.; Gossage, R. A.; Smeets, W. J. J.; Spek, A. L.; Van Koten, G. *J. Am. Chem. Soc.* **1997**, *119*, 11317−11318.
(77) Gusev, D. G.; Madott, M.; Dolgushin, F. M.; Lyssenko, K. A.; Antipin, M. Y. *Organometallics* **2000**, *19*, 1734−1739.
(78) Stępień, M.; Latos-Grażyński, L.; Szterenberg, L.; Panek, J.; Latajka, Z. *J. Am. Chem. Soc.* **2004**, *126*, 4566−4580.

DOI: 10.1021/jacs.7b13825
J. Am. Chem. Soc. 2018, 140, 3412−3422